Numerical and experimental investigation into the aerodynamic benefits of rotorcraft formation flight

Duivenvoorden, Ramon; Voskuijl, Mark; Morée, Lars; de Vries, Jan; van der Veen, Finbar

DOI
10.4050/JAHS.67.012011

Publication date
2020

Document Version
Final published version

Published in
American Helicopter Society. Journal

Numerical and Experimental Investigation into the Aerodynamic Benefits of Rotorcraft Formation Flight

Ramon Duivenvoorden*
Doctoral student
Delft University of Technology
Delft, the Netherlands

Mark Voskuijl
Professor
Netherlands Defence Academy
Den Helder, the Netherlands

Lars Morée
1st Lieutenant
Royal Netherlands Air Force
Woensdrecht, the Netherlands

Jan de Vries
Assistant Professor
Netherlands Defence Academy
Den Helder, the Netherlands

Finbar van der Veen
2nd Lieutenant
Royal Netherlands Air Force
Den Helder, the Netherlands

The use of formation flight to achieve aerodynamic benefit applied to rotorcraft has, unlike its fixed-wing counterpart, received little attention in the literature. This document presents a proof-of-concept of rotorcraft formation flight from two independent investigations: a numerical study of a fully articulated helicopter influenced by an upstream helicopter wake and a wind-tunnel experiment featuring two small-scale helicopter models with fixed-pitch blades. Both cases feature a representation of two helicopters in a diagonal, staggered formation aligned on the advancing side of the main rotor, but do not simulate directly comparable flight conditions. The vertical and lateral alignment of the two helicopters is varied in order to observe the achievable reductions in main rotor power required during cruise flight. The wind-tunnel experiment data yield an estimated maximum total power reduction for the secondary aircraft of approximately 24%, while the numerical models yield reductions between 20% and 34% dependent on flight velocity. Both experiments predict a higher potential for aerodynamic benefit than generally observed for fixed-wing formations, which is attributed to the asymmetric velocity profile induced by the wake of the upstream rotor. Optimal lateral alignment of both experimental and numerical results is found to feature overlap of the rotor disk areas, rather than tip-to-tip alignment, as a result of the circular rotor disk area. Experimental data show an optimal vertical alignment of the secondary rotorcraft below the primary, due to the self-induced vertical displacement of the rotor wake, which is absent from the numerical results due to the application of a flat wake assumption. The results show a promising potential for rotorcraft formation flight, though due to the limited nature of the models used, conclusions cannot be generalized. The potential aerodynamic benefit indicated by the present study invites further research in the field of rotorcraft formation flight.

Nomenclature

D	rotor diameter
M_θ, M_ϕ	pitch and roll moments
$P_{\text{req,MR}}$	main rotor power required
R	rotor radius
V	flight velocity

*Corresponding author; email:r.r.duivenvoorden@tudelft.nl
Previous version of paper presented at the VFS International 76th Annual Forum & Technology Display, Virginia Beach, VA, October 5–8, 2020. Awarded "Best paper in Aerodynamics Technical Session." Manuscript received October 2020; accepted August 2021.

$x/R, y/R, z/R$	coordinate with respect to (leader) rotor hub
$\beta_0, \beta_{1c}, \beta_{1s}$	flapping angles
$\Gamma(y)/\Gamma_0$	normalized vorticity distribution
$\theta_0, \theta_{1s}, \theta_{1c}, \theta_{0T}$	control angles
$\theta_{\text{body}}, \phi_{\text{body}}, \psi_{\text{body}}$	fuselage pitch, roll, and yaw angles
λ	induced velocity
μ	advance ratio

Introduction

The subject of formation flight for aerodynamic benefit has been thoroughly examined for both bird flight (e.g., Refs. 1, 2) and subsequently fixed-wing aircraft (e.g., Refs. 3–7), all leading to the conclusion that large reductions of induced drag are achievable across a formation of aircraft. The subject is, however, mostly untouched regarding rotary wing vehicles, although the increased interest in rotorcraft in recent years, such as through the emergence of urban air mobility, certainly merits its investigation.

Background

The main principle of formation flight for aerodynamic benefit, or "wake surfing," is the utilization of the upwash outboard of the wake of a primary aircraft by a secondary aircraft, which induces an additional angle of attack on the wing. The induced angle of attack has the primary effect that the lift vector is tilted forward and thus provides a component counteracting drag. Since its first characterization by Weiselberger in 1914 (Ref. 8) the subject of formation flight has matured from investigations on large formations of birds, most notably by Lissaman and Shollenberger (Ref. 1) and Hummel (Refs. 2, 9), to the application on full-scale passenger and cargo aircraft at practically feasible flight configurations, such as the extensive works by Ning et al. (Refs. 3, 10) and the experimental tests of NASA's Surfing Aircraft Vortices for Efficiency (SAVE) program (Ref. 4). All of these investigations consistently report induced drag reductions of the follower in a two-aircraft diagonal formation at longitudinal separations of at least 10 spans of roughly 30–50%, which translates to 10–15% of total drag reduction.

Considering rotorcraft, however, very little research has been published to date. A series of publications by Padfield et al. (Refs. 11–14) investigate the interaction of a helicopter with external wakes, focused on the handling qualities. They show that parallel wake encounters of helicopters with fixed-wing aircraft wakes in approach and landing conditions can have significant effect on handling properties. The wake encounters they consider, however, are of the scale of passenger aircraft and far exceed the scale of the helicopter itself. Furthermore, the approach and landing conditions considered do not feature high-speed forward flight, and it is difficult to interpret their results in the context of formation flight for aerodynamic benefit. A similar study by Matayoshi and Okuno (Ref. 15) suggest that at higher approach speeds (100 kt) the effect of wake encounters on handling qualities of helicopters may not be worse than those experienced by fixed-wing aircraft of equivalent size and weight.

A notable body of work exists on the subject of tiltrotors in formation flight, particularly focused on the V-22 Osprey (Refs. 16–19). In fact, the results presented by Johnson et al. (Ref. 16) show an increase in rotor thrust for a follower rotorcraft in formation when aligned to the outboard side of the leader wake, a first indication of the validity of the concept of formation flight for aerodynamic benefit applied to rotorcraft. The focus of these investigations is on potential performance degradation and the aforementioned increase in rotor thrust unfortunately lies on the edge of the investigated dataset and is not discussed specifically. Furthermore, the advance ratio is much lower than most utility helicopters in cruise conditions, since tiltrotors transition to fixed-wing mode for cruise. Silva et al. (Ref. 19) investigate a dynamic rolloff event caused by the interaction with the wake of an upstream aircraft, but the mechanism seems specific to the double tip-mounted rotor system of the V-22 Osprey. The rolling moment induced by a differential upwash between the two rotors, causing a differential thrust and thus a strong rolling moment based on the moment arms created by the wings. A single articulated rotor system would likely not respond in the same way. The only reference to single articulated rotors in formation found in the open literature, to the knowledge of the authors, is the work by Yeminici et al. (Ref. 20). They investigate helicopter rotors at relatively high forward speeds in staggered-diagonal formation, but again focus on the performance deterioration when the downstream rotor is positioned in the downwash of the upstream rotor. The extent of the considered alignment is not sufficient to shed light on potential performance benefits when aligned to the outboard side of the upstream rotor wake.

The lack of research on potential aerodynamic benefits from rotorcraft formation flight (RFF) is interesting, since the similarity between the rotary-wing and fixed-wing far wake is well documented, as early as 1954 (Ref. 21), and thus indicates that the formation flight mechanism may be applicable. Particularly the investigation by Heyson and Katzoff (Ref. 22) is a well-known reference, showing the development of a longitudinal vortex pair (or "supervortices") in the rotor wake in forward flight and therefore an outboard upwash region similar to that in fixed-wing wakes. They suggest the far wake is therefore best analyzed by an equivalent fixed-wing wake approach. Egolf (Ref. 23) analyses the rotor wake geometry and reaches a similar conclusion, with the addition that longitudinal vortex structures will form asymmetrically with a stronger concentration on the advancing side, as illustrated in Fig. 1. The asymmetry between the disk vortices is also present in the measurements by Heyson and Katzoff (Ref. 22) and can be seen in later high-fidelity simulations of the rotor wake, such as by Rajagopalan and Mathur (Ref. 24) and Caprace et al. (Ref. 25). The simulations by Caprace et al. (Ref. 25) particularly shows the asymmetry in the distribution of vorticity in the rotor wake and the higher concentration on the advancing side, which is maintained deep into the far wake, shown in Fig. 2. The observed asymmetry would suggest that the potential for aerodynamic benefit through wake surfing on a rotorcraft wake is dependent on the side of alignment, with the advancing side yielding a larger outboard upwash peak. Furthermore, compared to an equivalent (fixed-wing) symmetric wake, the rotor wake would yield a higher potential for wake surfing by aligning on the advancing side.

Methodology

As there is currently little to no research directly investigating the potential for rotorcraft wake surfing, a numerical simulation of RFF is developed in order to investigate the effects of a nonuniform induced velocity field, representative of the wake of an upstream helicopter, on a follower helicopter with an articulated rotor. The present study considers a diagonal, staggered formation aligned on the advancing side, based on the observations of the asymmetric wake vorticity distribution discussed in the Background section of this paper. The focus of the research is the change in performance of the follower rotorcraft due to the influence of the wake of the leader rotorcraft.

The numerical investigation is supplemented by an independently performed wind-tunnel experiment of small-scale helicopter models in formation. Like the numerical model, the wind-tunnel experiment considers two helicopters in a diagonal, staggered formation aligned on the advancing side of the leader rotor. In both the numerical simulations and the wind-tunnel experiments, longitudinal separation between the two helicopters is kept at a predefined distance, while lateral and vertical

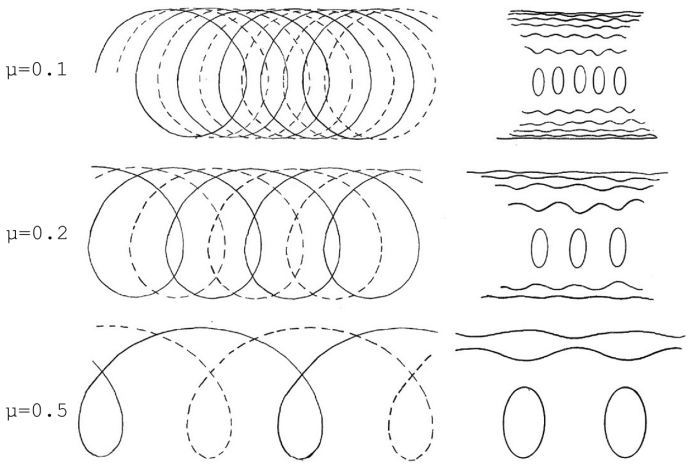

Fig. 1. Overlapping tip vortices of a rotor in forward flight (left) decomposed into far wake vortex structures (right). (Modified from Ref. 23).

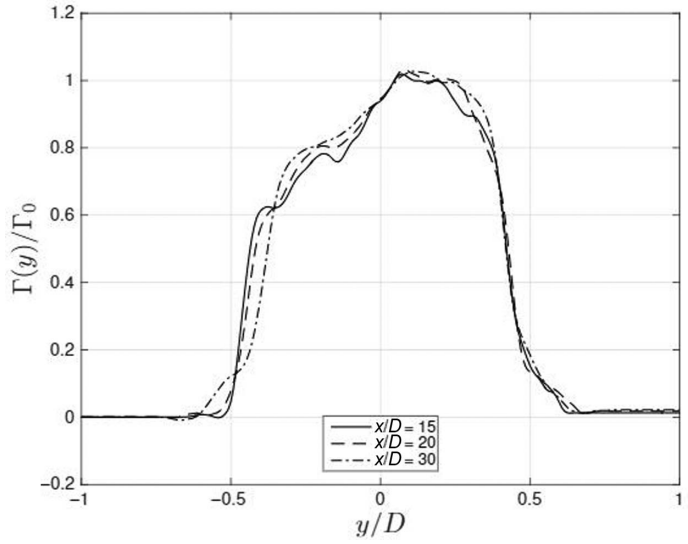

Fig. 2. Distribution of circulation in the wake at several downstream locations. Advancing side is represented by positive y/D (Ref. 25).

separation is varied in order to map the effects of formation flight as a function of formation alignment. The definition of relative distances is shown in Fig. 3 and used when reporting results for both the numerical simulations and wind-tunnel experiments.

Numerical methodology

The numerical simulations focus primarily on the follower rotorcraft, while simplifying the representation of the leader wake influence. Verification and validation of the components of the RFF model can be found in the Validation section of this paper.

Follower representation. The RFF model is built around the follower rotorcraft, the core of which is a rigid multibody dynamics (MBD) model built to behave like a typical helicopter. The MBD model closely resembles the UH-60 Black Hawk, utilizing data from Howlett (Refs. 27, 28), Ballin (Ref. 29) and Buckanin et al. (Ref. 30). The RFF model architecture is based on the MBD model originally developed by van Bruchem et al. (Ref. 31), in turn structured according to the approach proposed by Pastorelli et al. (Ref. 32). The MBD model includes representation of both nonrotating and rotating swashplate assemblies. Inflow on the blades is handled by a Peters–He inflow model, based on the equations from Ref. 33, run at 33 states (four harmonics and eight radial functions) as this is found to be an effective setup for higher advance ratios according to Peters and He (Ref. 34). Rotors are represented as rigid bodies and aerodynamic evaluation is handled by a blade–element method at 10 equiannular sections, with aerodynamic forces and moments taken from lookup tables of experimental airfoil data at appropriate Reynolds numbers. A single-point representation of the fuselage is included in order to close the MBD representation of the main rotor, with aerodynamic forces and moments on the fuselage based on the empirical model by Hilbert (Ref. 35).

In each simulation, the MBD model is initiated with a fixed rpm on the main rotor and free to move in 6 degrees-of-freedom. A "fly-to-trim" controller automatically adjusts control angles over time until the model reaches a steady-state flight condition at the predefined flight speed. When flying in formation, the follower is place in a fixed position within the induced velocity field of the leader wake, which is independent of the motion of the follower rotorcraft. The model thus forces the interaction of the follower with the leader wake and does not simulate the dynamic behavior of the follower when approaching the leader wake. All results in this paper are limited to the data captured after the follower has reached a trimmed, steady-state condition.

The aerodynamic lookup tables used in the RFF model are from experimental measurements of the NACA 0012, rather than the SC1095 and SC1094R8 airfoils of the UH-60 Black Hawk (Ref. 36), making the setup of the RFF very close to that of the FLIGHTLAB Generic Rotorcraft (FGR) model, which is used for verification purposes. The NACA 0012 airfoil tables used in the RFF model are taken directly from the FGR model. The FGR model also closely resembles the UH-60 Black Hawk, though it does not feature a full swashplate assembly like the RFF model. More information on FLIGHTLAB can be found in Refs. 37 and 38. Although the NACA 0012 differs from the actual airfoils used by the UH-60 Black Hawk, it is representative of a typical helicopter airfoil and thus fits the aim of the RFF model.

Leader representation. The influence of the leader rotorcraft is represented in a simplified manner. Rather than fully simulating another helicopter and its wake, the leader influence is based on a baseline simulation of the follower model. Blade loading from the baseline simulations is used as input for a flat wake model, which is in turn used to calculate induced velocity components at the location of the follower rotorcraft. The flat wake model was originally conceived by Baskin et al. (Ref. 39) as a quick estimation method for inflow on the rotor disk at advance ratios $\mu > 0.15$. It assumes the rotor to fully operate in edgewise flow, meaning it does not model the self-induced vertical displacement of the rotor wake. All vorticity is thus modeled on the $z/R = 0$ plane, similar to approaches in conceptual investigations of fixed-wing formation flight for aerodynamic benefit, which utilized distributed horseshoe vortices in order to represent the leader induced wake (e.g., Ref. 6).

The implementation of the flat wake method in the present research is strongly based on the DOWN code developed by NASA, which can be found in Ref. 40. Wilson (Ref. 41) gives an extensive validation study of this program, showing adequate correlation with experimental data on a level that is similar to other vortex methods at the time. Since the flat wake method is originally meant for estimations of inflow on the rotor disk, rather than in the far wake (Ref. 39), the present research includes additional comparison of the results of the flat wake method with the far wake measurement data from Heyson and Katzoff (Ref. 22), presented in the Validation section of this paper. The most important

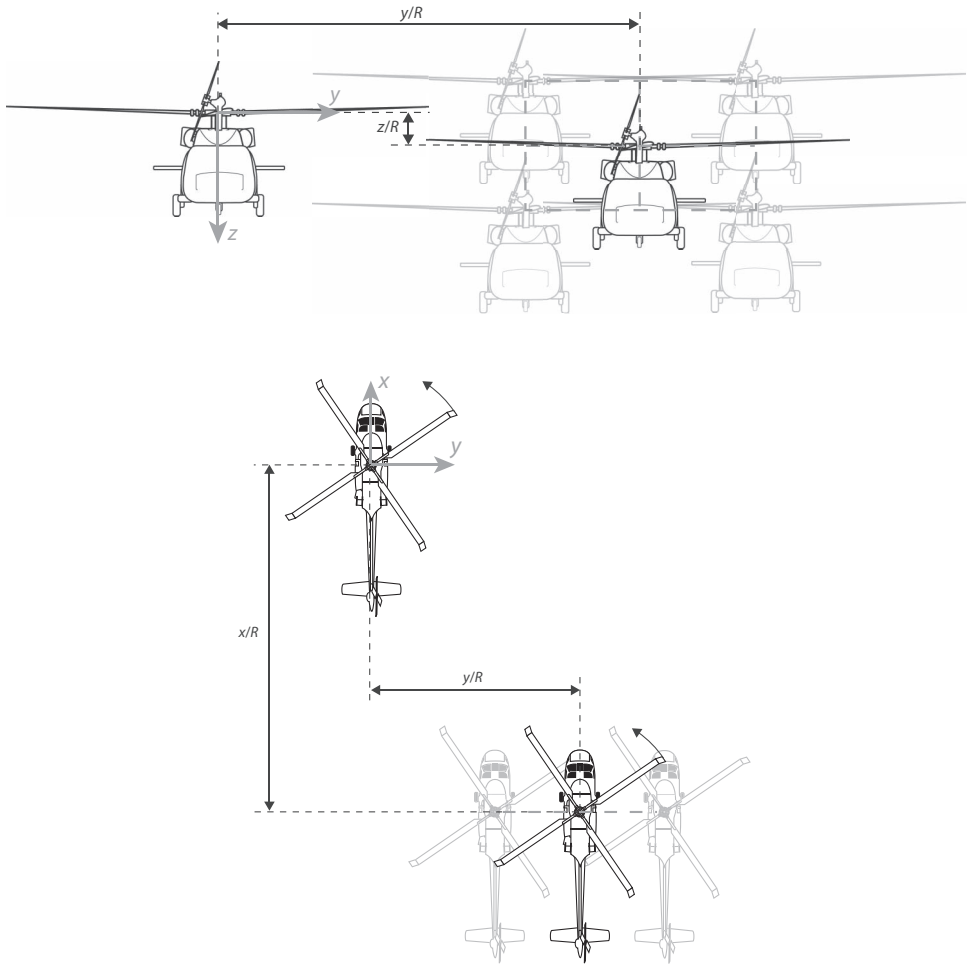

Fig. 3. Definition of relative positioning. (Blackhawk image source Ref. 26).

input for the flat wake model is the rotor blade vorticity distribution, which is extracted from a baseline solo-flight configuration of the follower rotorcraft model. There is no influence of the follower rotor on the leader rotor during simulation, which offers the option of generating a three-dimensional (3D) leader wake velocity field out-of-the-loop. Applying a range of $(-6<x/R<-4;\ 0<y/R<5;\ -1<z/R<1)$ at a resolution of 0.01, the generated velocity field captures the possible blade positions for all simulated formation alignments with negligible loss of accuracy. The model can then interpolate and add the wake velocities to the aerodynamic evaluation points of the follower representation during simulation, which is more efficient than an in-the-loop evaluation for all evaluation points at each time step.

On the limitations of the leader representation. The choice for the flat wake method is a limited approach, as it does not incorporate self-induced vertical displacement of the wake, wake contraction, wake rollup, and differential wake skew of retreating and advancing side supervortices. However, the benefit of the flat wake method is that it is fully independent of the wake distance at which induced velocities are evaluated, while still capturing the asymmetrical induced velocity field inherent to rotor wakes. Focus is given to the simulation of appropriate blade motions in the follower representation, as well as a wide variety of flight conditions and formation alignments that can be simulated. Based on the results from Caprace et al. (Ref. 25), Rajagopalan and Mathur (Ref. 24), and the measurements by Heyson and Katzoff (Ref. 22), the (differential) skew of the supervortices is not expected to exceed small angles for the advance ratios investigated in this paper, meaning the effect of the flat wake assumption on the orientation of induced velocity vectors will be negligible. The minimum advance ratio considered in this paper is $\mu = 0.187$, which exceeds the minimum advance ratio given for the validity of the flat wake assumption by Baskin et al. (Ref. 39) and Wilson (Ref. 41) of $\mu > 0.15$ by a significant margin. The lack of vertical displacement of the wake will have to be taken into account when interpreting the results of the present paper.

Model integration. Figure 4 gives a summary of the different modules used in the numerical simulation and the exchange of information between them. The calculation of the leader induced wake out-of-loop is a necessity in terms of computational resources, since the fly-to-trim method of the follower representation requires several thousand time steps for each simulation in order to converge to a steady-state flight. An in-the-loop evaluation was found to be too expensive compared to the out-of-loop approach, meaning it cannot account for mutual deformation of the leader and follower wake structures. Whitehouse and Brown (Ref. 42) perform a study on the validity of the one-way interaction (or "frozen vortex") approach and find that while it is inadequate for low-speed and hovering applications, it is less critical in the evaluation of rotor performance at high-speed forward flight than it is for lower flight velocities. As the present study considers a wider range of flight conditions and formation alignments, and considering the model architecture, preference was given to a one-way interaction approach.

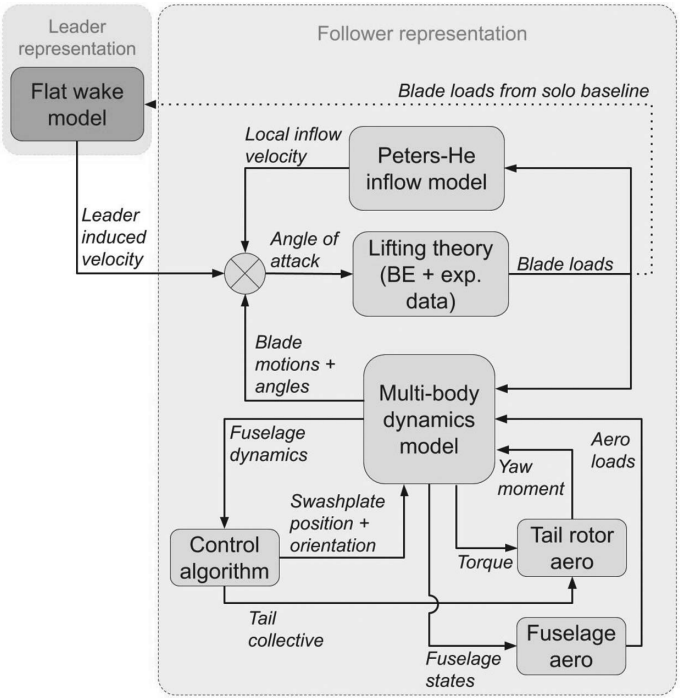

Fig. 4. Flowchart of the overall formation modeling. The dotted line represents an out-of-the-loop input based on a baseline calculation.

Table 1. Test matrix of numerical simulations

Run	FW Model	Mass (%)	Velocity (kt)	y/R	z/R
1	Off	100	110.8	–	–
2	Off	70–100	110.8	–	–
3	Off	100	80–120	–	–
4	On	100	110.8	1–3	−0.5 to 0.5
5	On	70–100	110.8	1.4–2	−0.3 to 0.3
6	On	100	80–120	1.4–2	−0.3 to 0.3

Test matrix. The numerical model resulting from the combination of the leader and follower representations, according to Fig. 4, is used to test the effects of formation flight on the secondary rotorcraft in various flight configurations. The primary dataset is taken at 110.8 kt ($\mu = 0.259$), which corresponds to the maximum range velocity calculated from the secondary rotorcraft model power curve. For the primary dataset, both leader and follower total vehicle weight are at roughly Maximum Take-Off Weight (MTOW) (see Table 5). Subsequently, the fuselage mass of the follower rotorcraft is varied in order to simulate the effects of variations in payload and fuel capacity. In terms of total vehicle mass, the variations range roughly from Operational Empty Weight (OEW) to MTOW. As the leader experiences no change in these configurations, the same baseline vorticity distribution is used for the flat wake method in these scenarios. Furthermore, the velocity of the entire formation (at the MTOW configuration) is varied between 80 and 120 kt ($\mu = 0.187$ and 0.281, respectively) in order to observe changes in optimal flight velocity. Here, the vorticity distribution for the flat wake method is extracted from a separate baseline for each velocity. In all cases, the position of the follower relative to the leader is varied both vertically and laterally while the longitudinal distance is kept at $x/R = -5$, yielding a two-dimensional map of data. From these, the optimal regions in terms of power required, control angles and positional stability are extracted.

Table 2. Tested mass percentages and absolute values of follower

Mass (%)	Fuselage (kg)	Total (kg)
70	4835	5367
80	5526	6058
90	6216	6748
100	6907	7439

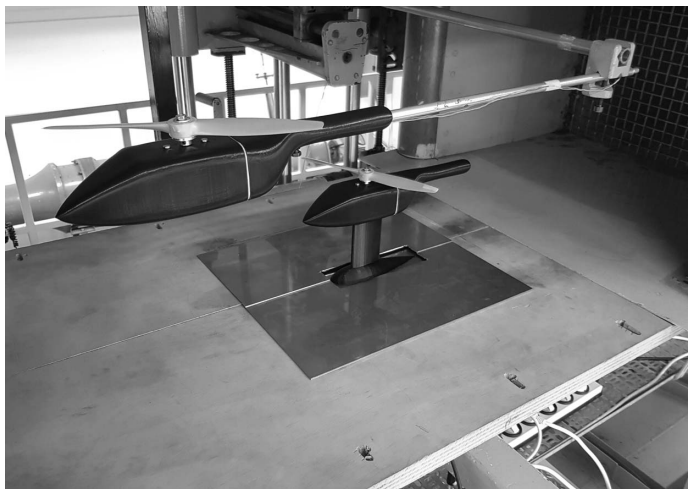

Fig. 5. Experimental test setup.

The full test matrix for the numerical simulations is shown in Table 1. The first three runs consist of the baselines for the formation flight sequences, evaluating the effects of a variety of fuselage mass and flight speed on the performance of the helicopter in solo flight. The flat wake model simulating the leader helicopter is turned off for these simulations. Table 2 yields the masses that correspond to the percentages reported in Table 1. Run 4 of Table 1 is the primary simulation, yielding the effects of formation flight on the follower helicopter performance at the solo maximum range velocity. Simulations are run for a wide range of horizontal and vertical alignments, as indicated, at intervals of 0.05. Runs 5 and 6 vary follower fuselage mass and formation flight speed, respectively, each at intervals of 10. Run 6 utilizes the results of Run 3 as input for the leader wake simulation.

Experimental methodology

The data from the numerical simulations are supplemented with wind-tunnel experiments performed at the Netherlands Defence Academy. These involve 3D printed scale-models fitted with fixed-pitch propellers, as shown in Fig. 5. Rotor thrust is controlled by varying power supplied to the electric motors, which changes the rotor rpm and thereby controls the generated thrust. The fuselages are 3D-printed from polylactic acid and are based on the NASA Rotor Body Interaction (ROBIN) model, specifically the ROBIN-Mod7 (Ref. 43). They have a length of 28 cm, with a hull width of 5.3 cm and a height of 4.5 cm. The tail boom is 15 cm long with a diameter of 2.0 cm. Measurements are taken at a wind-tunnel velocity of 9 m/s.

The follower helicopter is positioned at a fixed location in the wind tunnel, attached to a six component balance to measure forces and moments on the model. The leader helicopter can be freely positioned relative to the position of the follower to simulate the different formation alignments. The relative position between follower and leader can be

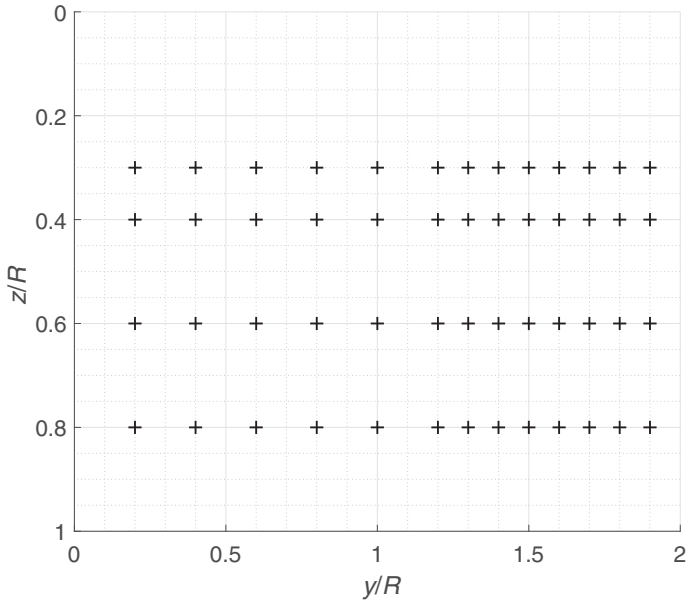

Fig. 6. Experimental measurement points.

varied laterally and vertically while the longitudinal position is kept at $x/R = 2$ due to geometrical constraints of the test section. The distribution of measurement points is shown in Fig. 6. Note that although the leader helicopter position was varied in the wind tunnel tests, rather than the follower helicopter, the positions are reported in the present study relative to the leader hub position, as to agree with the definitions of formation alignment given in Fig. 3.

Baseline measurements of a single helicopter are performed with the follower helicopter, where the wind tunnel is set to a fixed velocity and power supplied to the rotor is adjusted until vertical equilibrium (trim) is reached, corresponding to a thrust value of 1.8 N. Wind tunnel velocity is measured by use of a pitot tube. A tachometer, combined with frequency analysis of the measured forces on the balance, is used to determine rotor rpm, which are checked to yield identical results. The force balance is used to measure the torque applied on the rotor. Power is then calculated from the rotor torque and rpm. Additionally, power supplied to the electrical motor is measured and used to verify the measured rotor power through a numerical model of the motor.

For each of the formation flight measurements, the wind tunnel is set to a fixed speed after which the leader helicopter is put at a specific position. The power setting resulting from the baseline measurements is then applied to the leader helicopter motor as a fixed value. Subsequently, the follower rotor power supplied is varied until vertical equilibrium is reached. Main rotor power is then calculated and verified in the same manner as for the baseline measurements.

Verification and Validation

In order to place confidence in the results of the RFF model, several steps of verification and validation are performed. The follower representation within the RFF model, being an intricate combination of well-known and validated theories and models, is verified for its computational methods and implementation. Furthermore, the flat wake method is meant as a fast estimation method for the inflow on the rotor disk, rather than induced velocity fields in the far wake. Therefore, it is validated that its simulations of far wake induced velocities are adequate for the purposes of this research.

Follower

The RFF model shares much of its main computational structure and components with the commercial software Flightlab. Flightlab includes the FGR model, which shares most of its setup with the RFF model, including its resemblance of the UH-60 Black Hawk with the exception of the blade airfoil, which use NACA 0012 profiles. However, whereas the RFF model simulates both rotating and nonrotating swashplate assemblies, the FGR has no multibody representation of this assembly. The FGR model is used to verify the calculations of the follower representation in the RFF model. Figure 7 shows the angle of attack experienced by one of the blades during one rotation in trimmed condition, showing

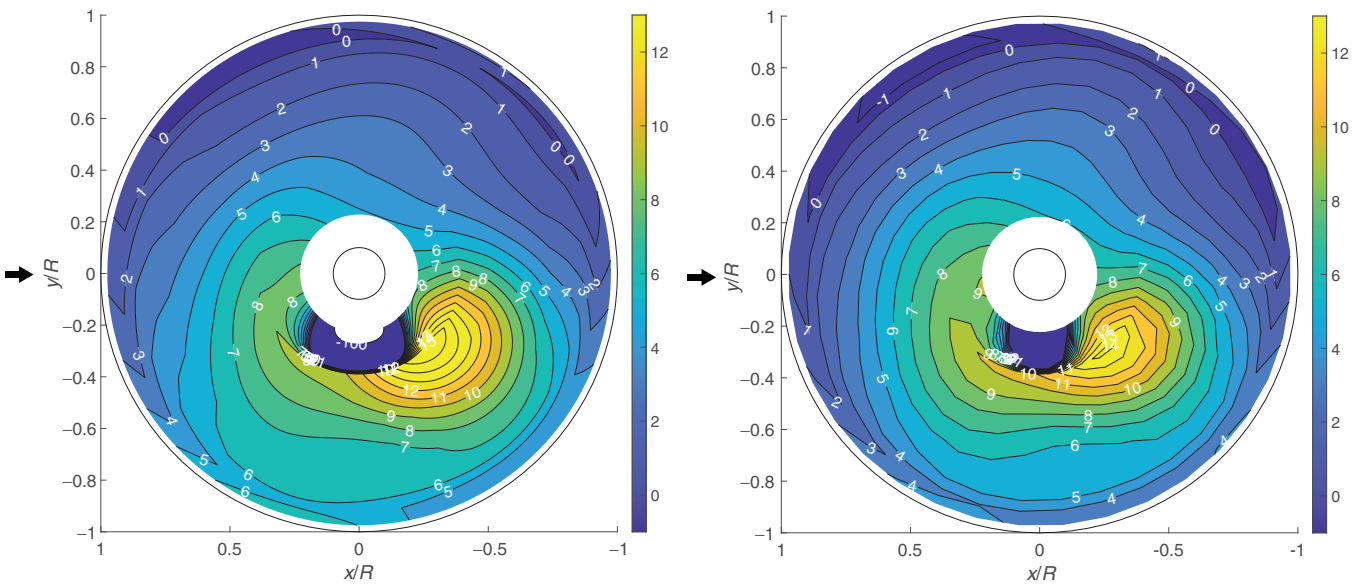

(a) Flightlab **(b) RFF model**

Fig. 7. Comparison of locally observed angle of attack in degrees on the rotor disk. Arrow indicates freestream direction.

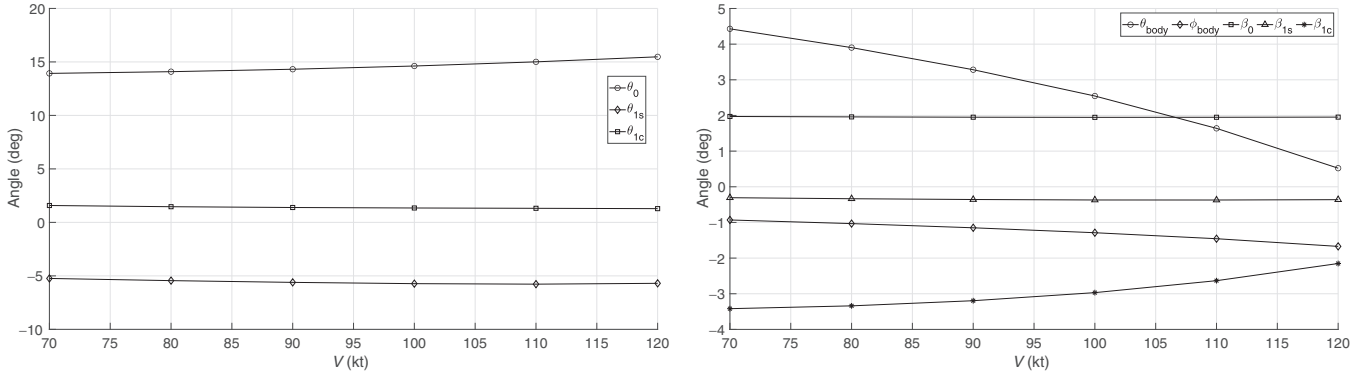

(a) Control angles (b) Body and flap angles

Fig. 8. Control, body, and flapping angles in trimmed condition (solo flight) as a function of flight velocity.

Table 3. Comparison of steady-state control, blade, and body angles between Flightlab reference and follower model

Variable (deg)	Flightlab	RFF Model
θ_0	16.56	15.04
θ_{1s}	−5.91	−5.76
θ_{1c}	2.11	1.31
θ_{0T}	10.21	17.96
β_0	2.73	1.95
β_{1s}	−0.33	−0.41
β_{1c}	1.95	2.65
θ_{body}	0.42	1.56
ϕ_{body}	−1.54	−1.47
ψ_{body}	−1.56E−4	−5E−4

close correlation in both distribution and magnitude. As the modules of the model all affect each other, rather than being a linear process, the distribution of the angle of attack over the disk can be viewed as the convergence of all states of the model. Agreement with the FGR model and thereby typical helicopter behavior is further exemplified by Table 3, which compares the control and body angles in trimmed condition between Flightlab and the RFF model. reasonable agreement for all parameters except for the tail rotor pitch angle is found. As the tail rotor is only used to maintain body orientation and has no aerodynamic link to the main rotor, the observed difference is of no consequence to the results of the RFF model.

Small differences between the Flightlab results and the RFF model are to be expected, since the models are highly similar but not identical. The FGR model uses a Bailey rotor model, whereas the RFF model utilizes a slightly more advanced version, as originally implemented by Voskuij et al. (Ref. 31). As noted, the tail rotor performance has no influence on the simulation of the main rotor performance and is only used to maintain body angle. The differences in the swashplate assemblies, which are fully modeled in the RFF model but not present in the FGR model, are another critical difference. Furthermore, although all setting such as number of states are matched between the Peters–He inflow methods used by both the FGR and RFF models, the authors cannot verify the exact code implementation of the Peters–He model in Flightlab, of which many versions and additions have been made since its conception. The RFF model uses the exact formulation given in Peters and He (Ref. 33). Considering the differences in the models, the values shown in Table 3 yields confidence in the behavior of the RFF model. Figure 8 furthermore shows the control, body, and flapping angles of the RFF model as a function of flight speed, which follow expected trends.

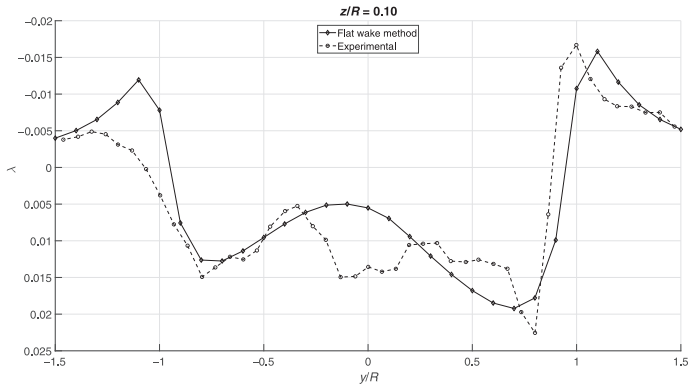

Fig. 9. Vertical induced velocity λ as predicted by the flat wake method versus measurements ($x/R = -3.14$). Axes defined according to Fig. 3.

Leader

The representation of the leader wake by means of the flat wake method by Baskin et al. (Ref. 39) warrants additional validation, since the model is originally meant as a model for inflow on the rotor disk. Utilizing it to estimate induced velocities in the far wake is, to the knowledge of the authors, a first. Though Wilson (Ref. 41) has performed a thorough correlation study on the theory, noting in particular the modeling of the asymmetric induced velocity distribution between retreating and advancing side as a redeeming feature compared to other analytical models of the time, all correlation data considered is located on or close to the rotor disk. When it comes to the downstream wake, the validation by Wilson (Ref. 41) does not guarantee performance of the model. Takahashi (Ref. 44) does use the flat wake model for the purpose of estimating downstream induced velocities, namely from the main rotor on the tail rotor. The streamwise distance from the main rotor considered is, however, not representative for the downstream stations considered in the present research. An additional validation phase of the flat wake method at further downstream distances is therefore presented in the present paper. As data on the far wake aerodynamics of rotorcraft in high-speed forward flight is scarce, the dataset of Heyson and Katzoff (Ref. 22) is used for this purpose. The measurement data include the induced velocity in the z-direction at $x/R = -3.14$, more than a diameter behind the rotor. Validation at this distance is deemed adequate for the longitudinal separation used in the numerical simulation ($x/R = -5$) based on the observation that most of the wake deflection and rollup occurs within one diameter behind the rotor (Ref. 22).

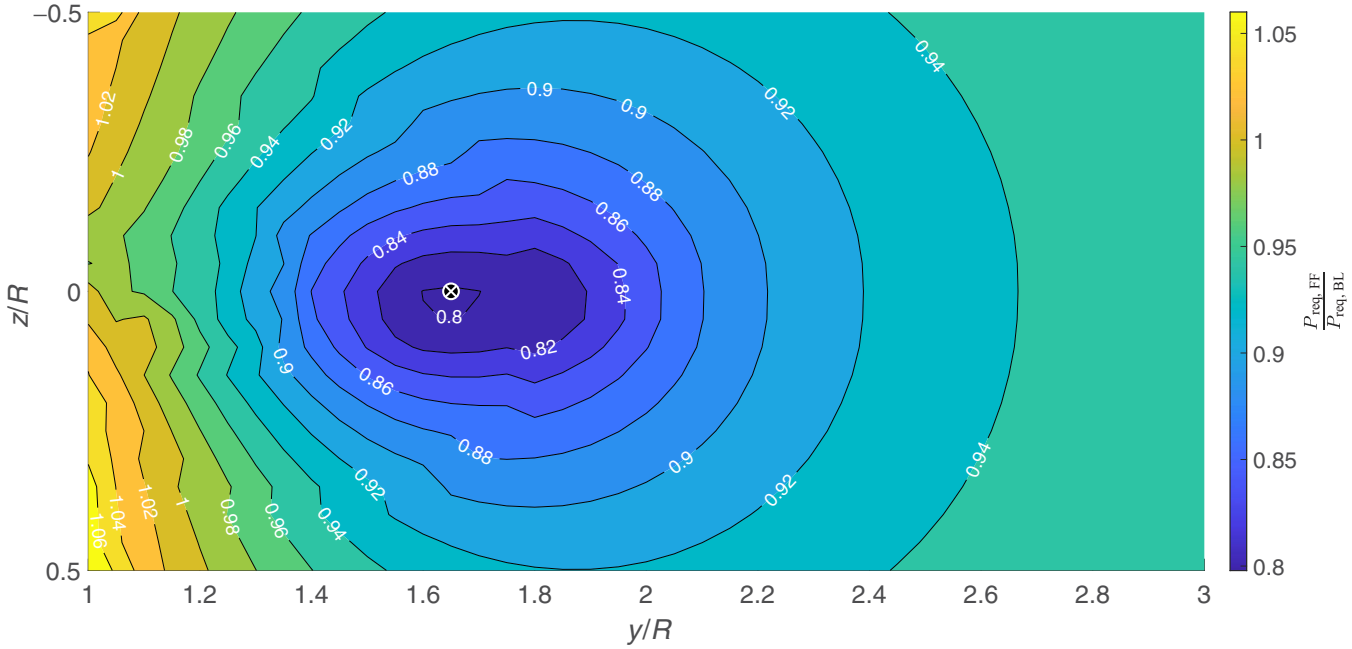

Fig. 10. Follower main rotor power required in formation as a fraction of the baseline value ($P_{\text{req,BL}} = 677\,\text{kW}$). Indicator gives location of minimum power fraction. Numerical simulation.

Figure 9 shows a comparison of the vertical induced velocity, which is the main variable of importance to formation flight effects, as predicted by the flat wake method compared to measurements made by Heyson and Katzoff (Ref. 22). Measurements are taken at a vertical position of $z/R = 0.10$ and include outboard lateral positions on both the advancing (right) and retreating (left) sides. The flat wake calculations are generated using inputs to match the rotor design, operating conditions and downstream measurement location of the experiment by Heyson and Katzoff (Ref. 22) ($x/R = -3.14$), obtained using the method presented by Baskin et al. (Ref. 39) in the same document where they establish the flat wake theory. Figure 9 shows that the flat wake method is able to predict the general trend and order of magnitude of the experimental measurements, though local variations are not captured. The asymmetry in induced velocity distribution between advancing and retreating sides is clearly visible in both the predicted and experimental data, which is an important characteristic of the flat wake method, as also noted by Wilson (Ref. 41). The correlation of the flat wake prediction is notably better on the advancing side than the retreating side. The discrepancy is seen in comparisons at other stations as well and is in line with observations made by Wilson (Ref. 41) in their validation efforts and follows expectations based on numerical simulations that show a diffuse supervortex on the retreating side and a concentrated supervortex on the advancing side (e.g., Ref. 25) which would result in less pronounced peaks in the retreating side induced velocities. Since the formation is aligned on the advancing side, the discrepancy of the induced velocity peaks on the retreating side is not considered a significant issue for the present study.

Results

This section presents the results of the completed RFF model, in which the MBD based follower model is subjected to the effects of the leader wake. Analyses of the effects of formation flight on power required, trim controls/moments, and static positional stability are presented.

Numerical simulation

In contrast to the fixed-wing formation flight research, where aerodynamic benefit of formation flight is quantified in terms of the reduction of induced drag, the effect of formation flight on the performance of rotorcraft is best viewed from the main rotor power required. The main result of the numerical simulation is therefore the fraction of main rotor power required in formation compared to the baseline value at various positions of formation flight. Furthermore, preliminary findings on control and stability, as well as the effects of payload mass and formation flight velocity, are presented. Because the RFF model includes aerodynamic drag of both blades and fuselage in its simulation, the main rotor power required can be interpreted as proportional to total aircraft drag in fixed-wing formation flight studies.

Power required. Figure 10 shows the fraction of follower main rotor power required in formation versus solo flight. The axes represent the lateral and vertical distance between the rotor hubs of leader and follower rotor, as defined in Fig. 3. Figure 10 shows a maximum power reduction of about 20%, which is a significantly higher number than observed in fixed-wing formation flight research, where total aircraft drag reductions typically ranges between 10% and 15%. The higher power reduction can be attributed to the increased potential of wake energy extraction due to the asymmetric vorticity distribution (and thus higher induced velocity concentration on the advancing side of the rotor) as noted in the Background section of the present paper.

The optimum position in terms of benefit to main rotor power required is indicated in Fig. 10 and found to be $(y/R, z/R) = (1.65, 0)$. Note that the vertical location of $z/R = 0$ is an artifact of the flat wake model and its lack of self-induced vertical displacement. At the station of maximum benefit to main rotor power required, a part of the follower disk area is positioned in the downwash region of the leader wake. Although it may be expected that this would lead to a reduction in performance, Fig. 11 illustrates how the circular disk area benefits more from an alignment in which the tip experiences downwash rather than upwash. In Fig. 11(b),

Table 4. Summary of required power and control data in and out of formation. Numerical simulation. Limits are taken from Howlett (Ref. 27)

	Power	Collective	Lateral Cyclic	Longitudinal Cyclic
Magnitude				
	(kW)	(deg)	(deg)	(deg)
Maximum	725	15.24	−1.34	7.38
Minimum	540	14.31	−1.22	5.40
Solo	677	15.04	−1.31	5.82
Limits	-	9.9:25.9	−8:8	−12.5:16.3
Fraction				
Maximum	1.071	1.013	1.060	1.269
Minimum	0.798	0.951	0.928	0.927
Position				
	$(y/R, z/R)$	$(y/R, z/R)$	$(y/R, z/R)$	$(y/R, z/R)$
Maximum	(1,0.5))	(1,-0.05)	(1.8,0.1)	(1,0)
Minimum	(1.65,0)	(1.7,0)	(1.25,-0.1)	(1.8,0)

the tip is aligned with the leader disk vortex, resulting in upwash on the entire disk. The maximum of the upwash is, however, only applied to a small area on the edge of the follower disk. Figure 11(c) represents the optimal alignment, where the tip experiences some downwash, but the peak of the upwash is applied to a much larger area of the disk, resulting in a higher reduction in main rotor power required. The optimal lateral alignment should therefore always be expected to feature some overlap, due to the interaction of the induced velocity distribution and the circular disk area, and may vary significantly with rotor design.

Control angles. Figure 12 shows the same two-dimensional maps as given in Fig. 10, but for the trim control variables as a fraction of their baseline value. A few notable observations can be made. The collective angle map is similar to the power fraction map, but their minima do not coincide, showing the dependency of the other control variables on the performance. The longitudinal cyclic is shown to have a strong lateral gradient, much more so than the lateral cyclic. This gradient shows the follower in the formation is mainly affected in pitch characteristics when in formation flight. An explanation for the pitch sensitivity is found in occurrence of phase lag. As the upwash from the leader wake is most effective on the retreating side of the follower disk, forces, and moments applied on the rotorcraft are delayed by a phase shift of approximately 90°, thus primarily affecting pitch behavior.

In general, the effect on the control angles required for trim is found to be mild. Though the maximum deviation of the longitudinal cyclic is 25%, it only occurs at the very edge of the range of alignments and still translates to a control setting well within the limits of the control system. The other control angles show even less deviation from their baseline value, as summarized together with the power data in Table 4. A final notable observation is that at the optimal position in terms of power, all control angles are reduced compared to their baseline value, meaning the formation flight effects counteract the moments experienced in solo flight.

Static positional stability. Taking the gradients from the control angle maps also yields insight into the static positional stability of the follower in the formation. The static positional stability is based on the moments that would act on the follower in trimmed condition under the influence of a small positional disturbance, without adjusting its controls. As the data are obtained in lateral and vertical directions, the ability of the follower to maintain its position in y- and z-directions can be found. The stability in the y-direction is dependent solely on the lateral cyclic control and can be considered statically stable if the gradient with respect to y is negative, as given by Eq. (1). Any disturbance in lateral position without adjusting control settings would then induce a moment counteracting the disturbance.

$$\frac{\delta\theta_{1c}}{\delta y} > 0 \tag{1}$$

$$\frac{\delta\theta_{1s}}{\delta z} < 0 \tag{2}$$

$$\frac{\delta\theta_{0}}{\delta z} > 0 \tag{3}$$

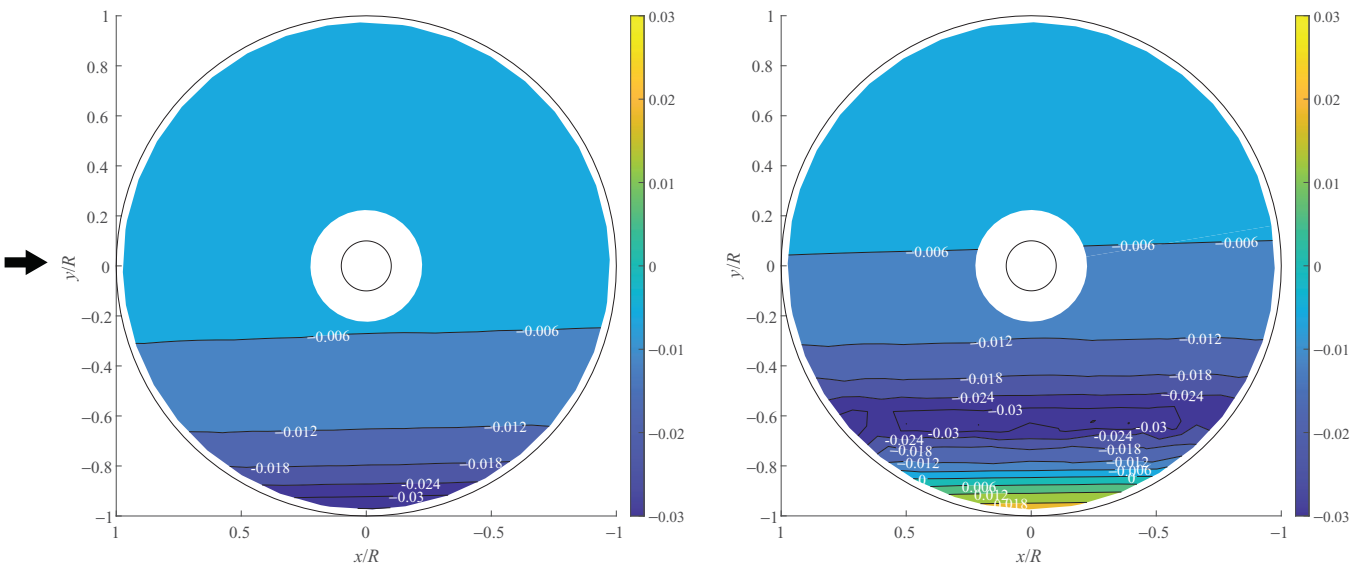

(a) $(x, y, z) = (-5R, 2R, 0)$ **(b) $(x, y, z) = (-5R, 1.65R, 0)$**

Fig. 11. Leader induced vertical inflow λ on the follower disk for "tip-to-tip" alignment (left) versus optimal alignment (right). Arrow indicates freestream direction. Numerical simulation, $x/R = -5$.

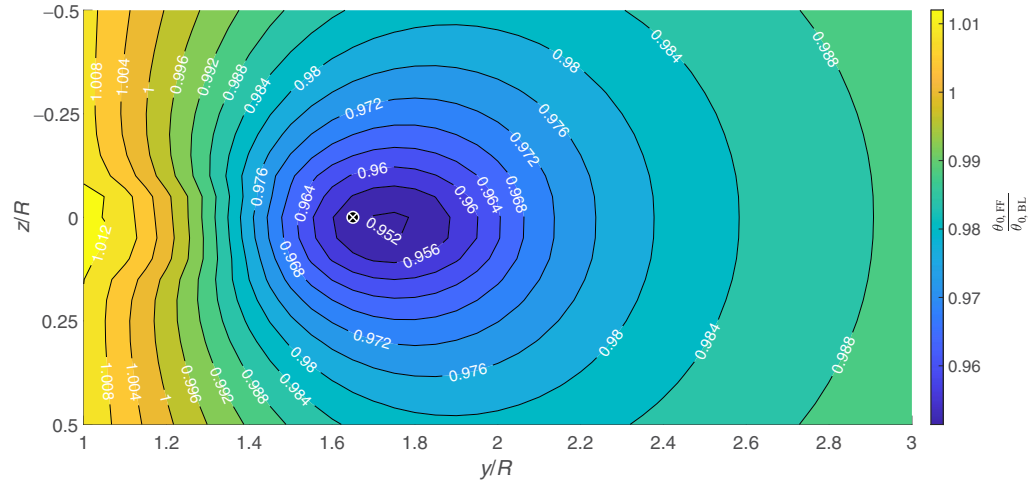

(a) Collective angle

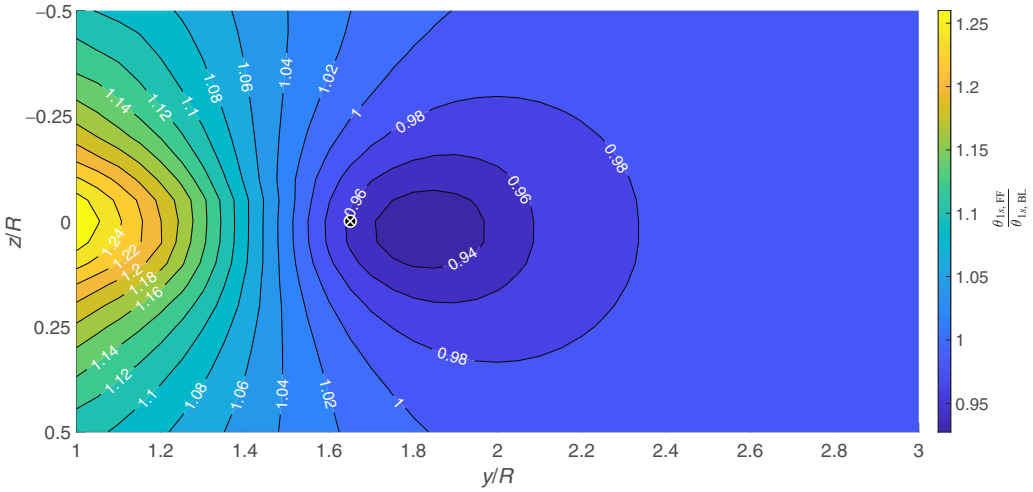

(b) Longitudinal cyclic

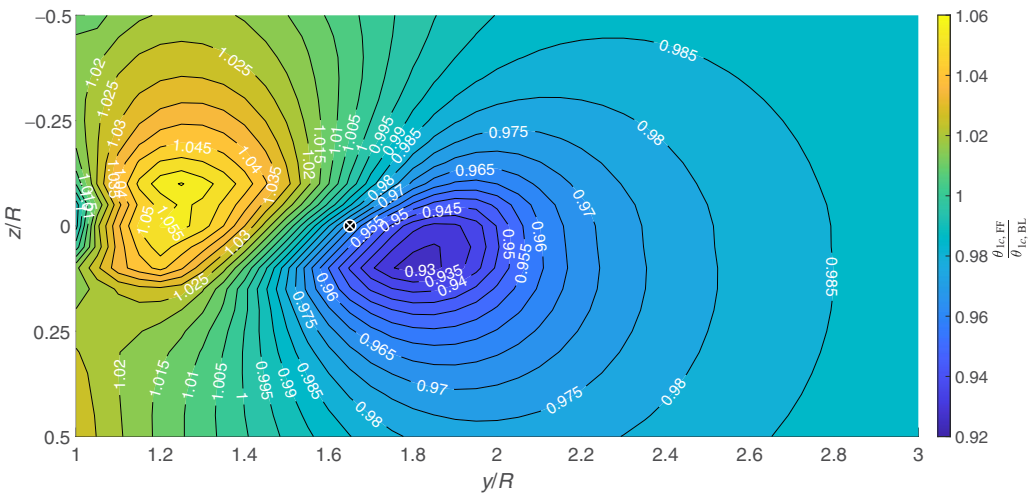

(c) Lateral cyclic

Fig. 12. Follower trim angle fractions as a function of alignment. Indicator gives location of minimum power fraction. Numerical simulation.

Table 5. Summary of effects of changing follower fuselage mass, $\mu = 0.26$. Numerical simulation

Mass (%)	70	80	90	100
$\Delta P_{req,MR}$ follower (%)	−17.5	−19.5	−21.1	−20.3
Position (y/R, z/R)	(1.5,0)	(1.6,0)	(1.7,0)	(1.65,0)

The stability in the z-direction is dependent on both the collective and longitudinal cyclic controls, according to Eqs. (3) and (2), respectively. Static positional stability in the z-direction requires both collective and longitudinal cyclic contributions to be statically stable. In the case of a single stable parameter, static stability is conditional on the relative influence of each parameter, which is not evaluated in the present research. Figure 13 indicates the positional stability of the follower at each position, plotted over the power fraction map.

Most of the region featuring a reduction in power is shown in Fig. 13(a) to be stable in the y-direction. As the follower is positioned further outboard, the position becomes unstable. The presented data cannot indicate the severity of the instability, though from the small gradient of the lateral cyclic angle found in Fig. 12(c) static instabilities are expected to be mild. The static stability of the optimum position strongly contrasts findings in fixed-wing formation flight, such as presented by Veldhuis et al. (Ref. 45), where the optimum is found to be unstable with respect to every control direction.

The static stability in the z-direction is found to be conditional for nearly every position, meaning that the actual static stability in the z-direction is dependent on the relative contributions of collective and longitudinal cyclic gradients. As with the lateral cyclic, however, the gradients observed in the control maps of Figs. 12(a) and 12(b) are small, particularly with respect to the z-direction, and instabilities are therefore expected to be mild.

Mass variations. The follower fuselage mass is varied between 70% and 100% of the primary simulation value, corresponding roughly to OEW and MTOW, respectively. These results can be used to determine the effects of variable payload between leader and follower. Leader is kept at constant mass (equal to the 100% follower mass setting) for all simulations. The simulations are carried out for lateral and vertical positions of $y/R = 1.4$–2 and $z/R = -0.5$ to 0.5; a subset of the primary simulation. Table 5 summarizes the maximum achieved reduction in power required for each mass variation, along with the corresponding position.

The correlation of follower fuselage mass and achieved power reduction in formation is shown to be nonlinear, with an optimum at 90% follower fuselage mass. Furthermore, the optimum position moves inboard as achievable power reduction decreases. These observations are likely tied to the stall region on the retreating blade, which is partly dependent on the collective control and thus on the required lift. Lower lift requirements will result in a less pronounced stall region, changing the balance of the circular disk area effect (Fig. 11) because of more effective root area. This allows for a more inboard position before the downwash on the tip region outweighs the upwash in the inboard regions. The nonlinearity with the mass percentage indicates, however, that there are multiple contributing effects.

Velocity variations. Changing the velocity of the formation reveals that the follower can achieve profoundly higher power reductions as the formation velocity decreases. Reducing the forward flight velocity increases the vertical induced velocity in the wake, which in turn leads to higher upwash peaks on the outside of the wake. These higher upwash peaks allow for a larger benefit to the follower. Table 6 gives the minimum

Table 6. Main rotor power required for varying flight speeds at a relative position of (y, z) = (1.65R, 0). Numerical simulation

Velocity (kt)	80	90	100	110	120
Advance ratio	0.186	0.210	0.232	0.256	0.279
$P_{req,MR}$ (solo) (kW)	544.7	579.1	625.6	686.4	768.3
$P_{req,MR}$ (follower) (kW)	359.3	409.4	472.1	537.8	636.5
$P_{req,MR}$ (averaged) (kW)	452.0	494.3	548.8	612.1	702.4

main rotor power required for the solo baseline, follower in formation and average of the formation. The follower power required in formation equals 359.3 kW at a flight speed of 80 kt ($\mu = 0.187$), a reduction of 34% compared to the baseline. When averaged over both rotorcraft in the formation, the maximum achievable power reduction is 17% at 80 kt ($\mu = 0.187$). It should be noted that the validity is strongly dependent on the flight speed, since the assumption of a 90° wake skew angle becomes increasingly invalid as the advance ratio decreases. The minimum advance ratio $\mu = 0.187$ considered in this study does not violate the minimum specified advance ratio for which the flat wake assumption is considered valid ($\mu = 0.15$).

Taking the power as directly proportional to the fuel consumption, the specific range can be estimated by dividing the flight velocity by the power required at that velocity. Figure 14 shows how the maximum range velocity is changed by formation flight. While the follower achieves the maximum specific range for the tested flight speeds at 80 kt, the leader performance is deteriorated as it experiences no effect of the formation flight, leading to a reduction in specific range averaged over the formation. The average of the total formation has a maximum around 100 kt ($\mu = 0.232$), compared to 110.8 kt ($\mu = 0.259$) for the solo baseline. The change in optimum flight speed for a formation as a whole is similarly noted for fixed wing aircraft, as reported in Ref. 5.

Wind-tunnel experiment

The results from the wind-tunnel experiment are reported in a similar manner to the numerical results. They include main rotor power required fraction, rolling and pitching moments (since there are no control angles for the rigid scale-model rotors) and positional stability.

Power required. Figure 15 shows a similar dataset to Fig. 10 of the numerical results, namely the main rotor power required of the follower in formation as a fraction of the baseline. The minimum power required is found to be 49% of the baseline value at $y/R = 1.3$ and $z/R = 0.6$, corresponding to a power reduction of 51%. The parasitic power requirement is not included in the measurements due to limitations in the experimental setup, but can be estimated using standard division of contributions to the power required corresponding to the tested advance ratio, as found in Prouty (Ref. 46). The equivalent total power reduction is then estimated to be approximately 24%. The nonuniformity of the power fraction map is attributed to the nonuniform distribution of the vortices at this longitudinal station of the leader wake, as can be inferred from the simulations by Caprace et al. (Ref. 25).

Pitch and roll moments. Figure 16 shows the change in measured pitching and rolling moments of the follower in formation from their baseline values (0.0295 and −0.0682 Nm, respectively). There are two main contributions to the observed variation in pitching moment. The first is the change in pitching moment due to the change of power required. As the power required scales with the rpm of the rotor, a lower power required will reduce the overall moment experienced by the rotor. The lateral variation of pitching moment is primarily caused by this effect. The vertical

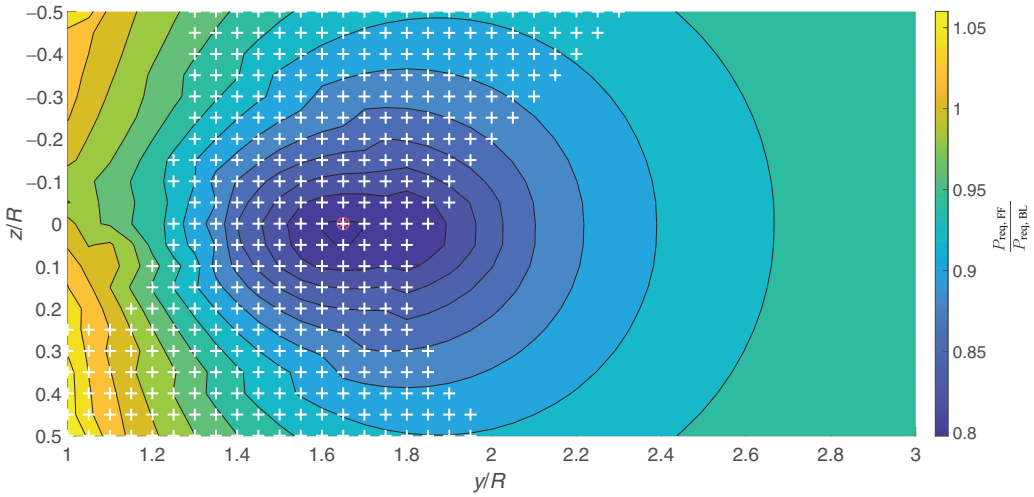

(a) Stability in y - Lateral cyclic

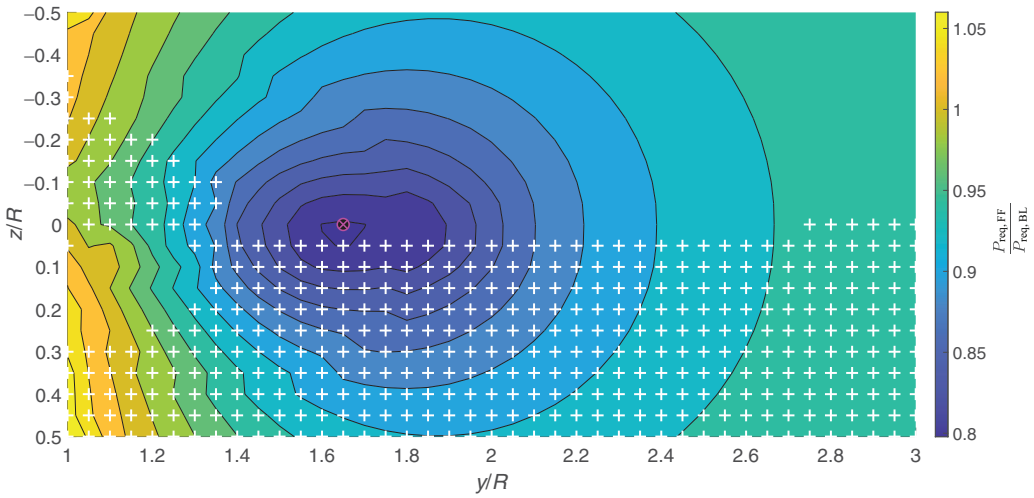

(b) Stability in z - Collective

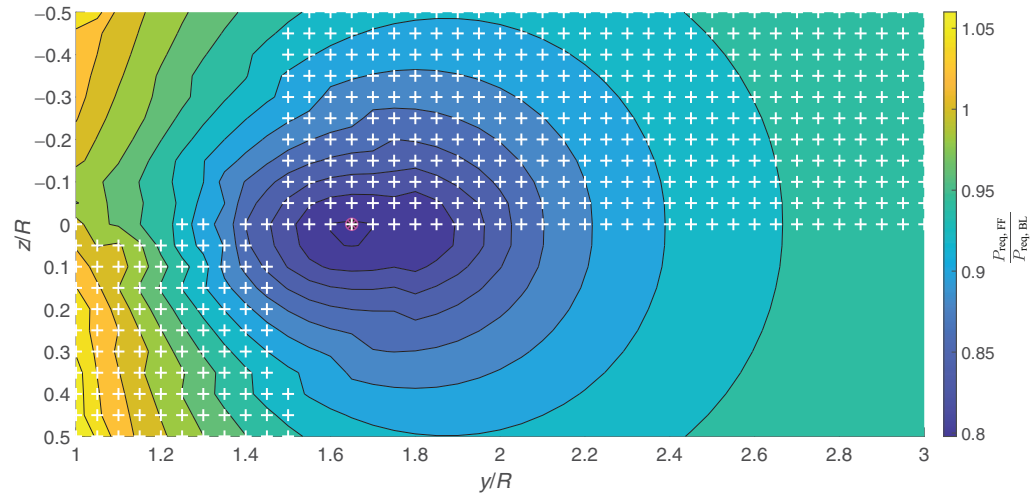

(c) Stability in z - Longitudinal cyclic

Fig. 13. Static positional stability in y- and z-direction of follower plotted over the main rotor power fraction. (+) marks stable conditions, unmarked areas are unstable. Minimum power fraction location is indicated. Numerical simulation.

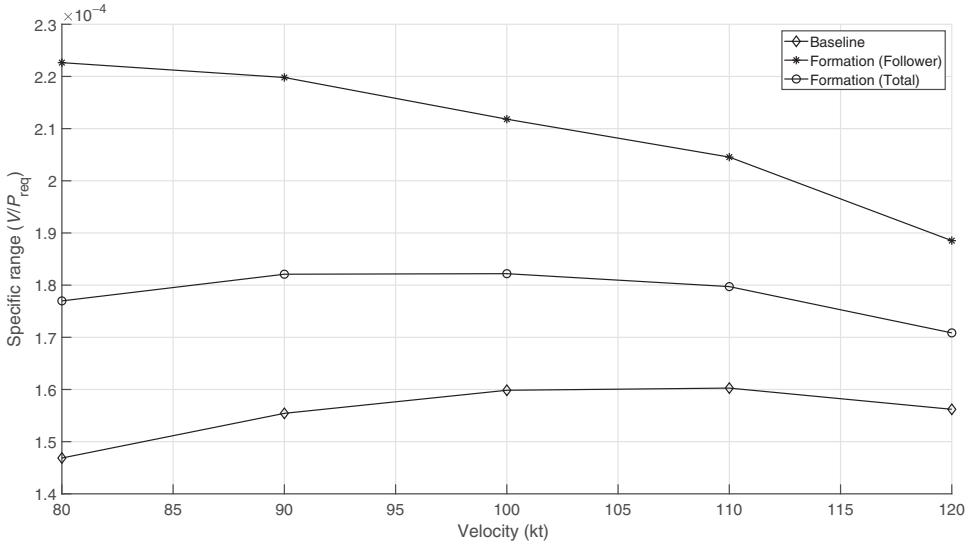

Fig. 14. Specific range curves for the baseline, follower in formation and total formation (averaged). Numerical simulation.

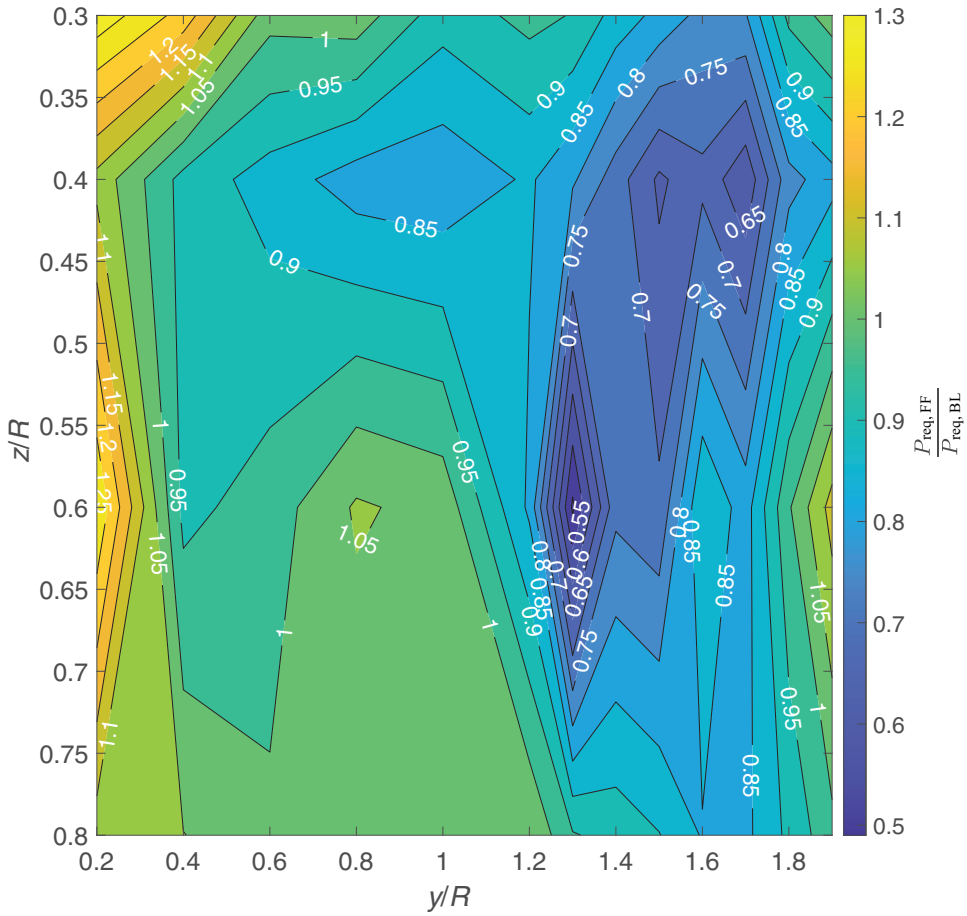

Fig. 15. Measured main rotor power required in formation as a fraction of the baseline. $\mu = 0.36$. Wind-tunnel measurement.

variation of the pitching moment, which is primarily present between lateral coordinates $y/R = 1$ and $y/R = 1.8$, can be attributed to the vertical displacement of the leader wake. Considering the downwash of the leader as a skewed cylinder and taking into account the short longitudinal distance between rotors, the front half of the follower rotor is immersed in the downwash when moved in the positive z-direction, causing additional pitch down moment and increasing the difference with the (pitch-up) baseline value.

The change in rolling moment, shown in Fig. 16(b), has a more complex distribution. Since the rpm scales with the power required and

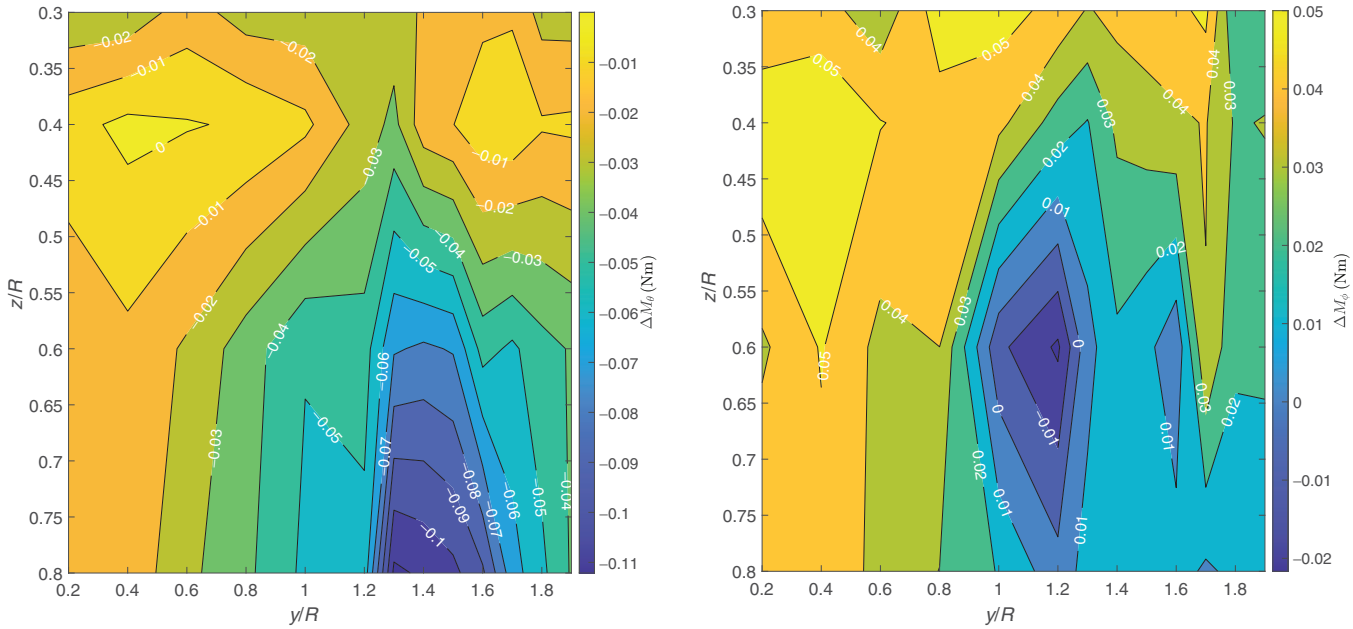

(a) Pitching moment (Nm) **(b) Rolling moment (Nm)**

Fig. 16. Measured change in moments experienced by the follower in formation. $\mu = 0.36$. Wind-tunnel measurement.

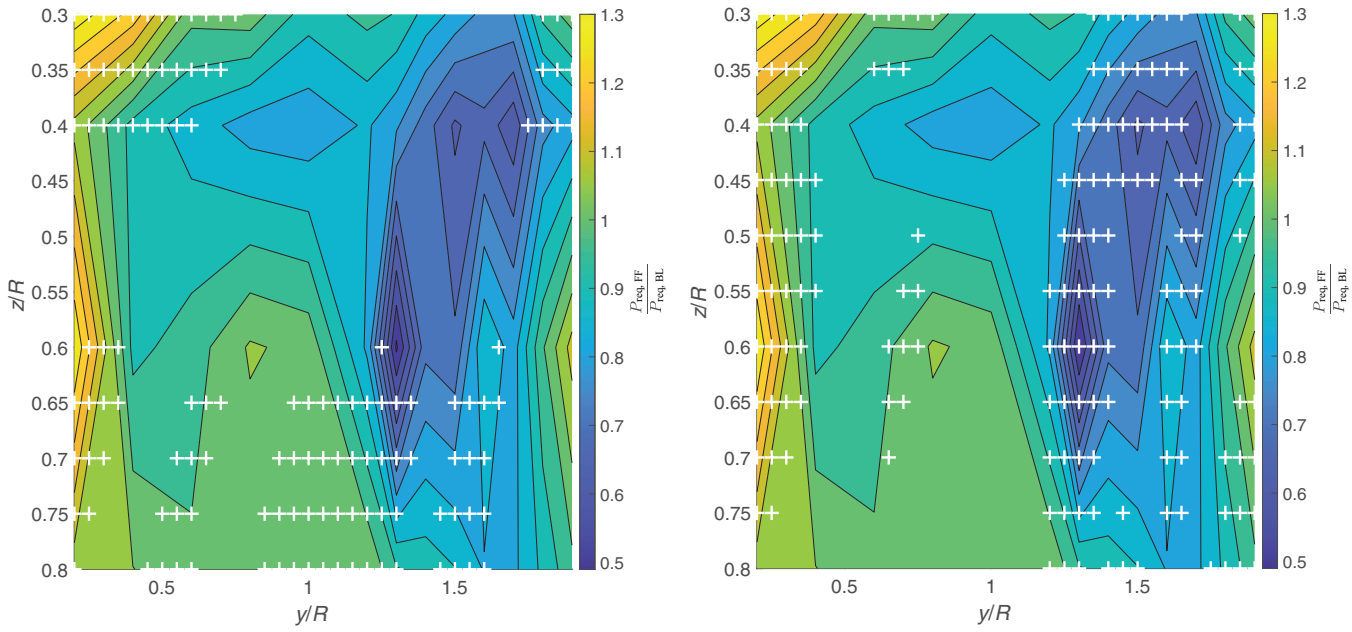

(a) Stability in z **(b) Stability in y**

Fig. 17. Stability in z- and y-direction plotted over power required fraction. $\mu = 0.36$. Stable areas denoted with (+) markers. Wind-tunnel measurement.

the rotors are fixed pitch, there is a strong dependency of the rolling moment on the power required. Though a similar dependency exists for the pitching moment, the effect on the roll moment is much stronger due to the forward velocity. Any station with lower power required in formation will therefore also exhibit a direct reduction of pitching moment, aside from any effect the leader wake has on the follower rotor. It is difficult to separate the dependency on power required from other effects when discussing Fig. 16(b); however, a few observations can be made. Overall, the rolling moment is increased compared to the baseline, apart from a minimum region around $y/R = 1.2$ and $z/R = 0.6$, where the rolling moment is reduced. This location is close to station for minimum power required, but does not fully coincide, showing that the position of the follower rotor relative to the leader wake is still significant. For $y/R < 1.2$, the distribution shows a tendency of increasing rolling moment with decreasing y/R. This tendency follows expectation as the follower rotor will experience more of the leader downwash on its retreating side, while the upwash peak is positioned further towards the advancing side tip. The particular location, where

maximum rolling moment is experienced by the follower, is found around $y/R = z/R = 0.4$. This location is dependent on the effective area of the up- and downwash peaks of the leader wake, similar to the effect shown in Fig. 11, and the moment arm to the hub. Finally, Fig. 16(b) shows increased roll moments at the stations around $y/R = 1.6$ and $z/R = 0.4$, even though the power required at these stations is strongly reduced, according to Fig. 15. This region of apparently strong rolling moment increase, as well as the overall higher rolling moments for lower z/R, are likely tied to the vertical shift of the leader wake and immersion of the follower rotor disk in said wake, similarly to the dependency described for the pitching moment.

The analysis of Figs. 16(a) and 16(b) furthermore reveals an essential difference between the articulated rotor of the follower in the numerical simulation, which is primarily affected by formation flight in its pitching moment due to phase lag, whereas the fixed rotors used in the experiment do not experience phase lag and are thus affected strongly in their rolling moment.

Static positional stability. From Figs. 16(a) and 16(b), an estimate of the static positional stability in y- and z-directions can be made. Moment gradients in y- and z-directions are, respectively, considered statically stable if the change in pitch and roll moment counteracts a positional disturbance, meaning the roll moment gradient has to be negative, while the pitching moment gradients have to be positive, as given in Eq. (4) for roll and Eq. (5) for pitch behavior. Note that these results do not include any insight into dynamic stability, which may be significantly affected by wake influence, but is not measured in this experiment.

$$\frac{\delta M_\phi}{\delta y} < 0 \tag{4}$$

$$\frac{\delta M_\theta}{\delta z} > 0 \tag{5}$$

Taking the gradient of the roll and pitching moments of Fig. 16 and applying Eqs. (4) and (5) then yields the static stability regions as shown in Figs. 17(a) and 17(b) for y- and z-directions, respectively. The markers indicate stable positions, plotted on the contour plot of the fraction of power required. Static stability in the y-direction is present for most of the region associated with the lowest power requirements. The z-direction shows static stability for most of the area below the minimum power required point ($y/R = 1.3$, $z/R = 0.6$), while the region above it is unstable.

Conclusions and Recommendations

This research investigates the conceptual validity of utilizing formation flight principles to reduce main rotor power required of rotorcraft. A numerical model resembling two UH-60 helicopters in diagonal leader–follower formation was created. The paper also presents results of an independent wind-tunnel experiment of two scale-model helicopters with the same objective. Numerical and experimental results are obtained under dissimilar operating conditions, making direct comparison impossible. However, both numerical and experimental research yields reductions of main rotor power required from aerodynamic benefit due to formation flight of the same order of magnitude. Furthermore, essential differences in the dependencies of moments on formation alignment are found between articulated and nonarticulated rotors.

The following main observations have been made in this research:

1) Both numerical and experimental investigations yield a positive proof of concept for the use of formation flight for aerodynamic benefit with rotorcraft.

2) At the baseline (solo flight) maximum range velocity, the numerical simulation yields a maximum achievable reduction of total power required through formation flight for the follower of 20%. Compensating the wind-tunnel results for the absence of parasitic drag yields an estimated 24% of the maximum total power required reduction for the follower in formation flight.

3) The achievable reductions in power required are higher than seen in fixed wing research, both in the numerical and experimental case. This can be attributed to the asymmetric nature of the rotor wake in forward flight, meaning rotorcraft may have a higher potential for aerodynamic benefit when aligned on the advancing side of the leader rotor.

4) In the numerical simulation, the optimal alignment in formation resulted in lower required trim settings for the follower compared to solo flight.

5) According to the numerical results, the maximum range flight speed when considering the formation as a whole is reduced compared to solo flight.

6) In the numerical experiment, the follower is statically stable in the y-direction and conditionally statically stable in the z-direction in the region of maximum power reduction.

7) In the wind-tunnel experiment, the results shows a more distributed area of strong power reduction. The positional static stability characteristics are similar to the numerical results.

It is important to note here that the conclusions of this paper are based on elementary models and experiments, which lack many (aero)dynamic effects that may change the observed behavior. This research is meant to provide a preliminary insight into the validity of the concept of formation flight for aerodynamic benefit as applied to rotary-wing vehicles, which is to say that the conclusions cannot be generalized without significant further investigation.

Recommendations

In light of the elementary nature of the presented investigation, the authors give several recommendations for the continued pursuit of this subject.

1) In order to investigate the effects of 3D flow phenomena, the RFF model should be fitted with a more advanced leader wake simulation. The inclusion of a free wake model for both leader and follower representation, including two-way interaction, would be recommended for more detailed simulation of the system.

2) A study to prove and quantify the hypothesis of alignment side sensitivity of potential aerodynamic benefit would be appropriate. This should include a more advanced leader representation, as the retreating side vorticity is significantly more distributed than the advancing side, as seen in simulations of far wake structures (e.g., Ref. 25).

3) Another important aerodynamic improvement would be to include fuselage interference effects. Both the effect of the leader wake on the fuselage as well as the fuselage on the main rotor would be of interest.

4) The series of publications on helicopter handling qualities in parallel wake encounters (Refs. 11–14) suggest that the flight dynamics situation may be significantly different from the static stability observed in this research and should be investigated.

5) The recent research by Caprace et al. (Ref. 25) discusses the concept of far wake strengthening, which seems to be supported indirectly by other sources, such as the investigations on tilt-rotor vehicle interference by Johnson et al. (Ref. 16). This phenomenon may raise achievable drag reductions at larger longitudinal separations significantly and warrants further investigation.

6) The collected numerical data on the variations of fuselage mass and formation velocity can be used to perform a first estimate of mission-specific achievable benefits of formation flight.

7) Aerodynamic measurements of two rotors in formation can yield insight into the wake interaction and whether the wake asymmetry between advancing and retreating side persists for larger formations.

8) The nonlinear behavior of achievable power reduction with follower fuselage mass warrants additional investigation.

For further inquiries on the available data or further specification of the models, please contact the authors:
Ramon Duivenvoorden (r.r.duivenvoorden@tudelft.nl),
Mark Voskuijl (M.Voskuijl@mindef.nl).

References

[1]Lissaman, P. B. S., and Shollenberger, C. A., "Formation Flight of Birds," *Science*, Vol. 168, 1970, pp. 1003–1006.

[2]Hummel, D., "Aerodynamic Aspects of Formation Flight in Birds," *Journal of Theoretical Biology*, Vol. 104, (3), October 1983, pp. 321–347. DOI: 10.1016/0022-5193(83)90110-8.

[3]Ning, A., Flanzer, T. C., and Kroo, I. M., "Aerodynamic Performance of Extended Formation Flight," *Journal of Aircraft*, Vol. 48, (3), May 2011, pp. 855–865. DOI: 10.2514/1.C031046.

[4]Bieniawski, S. R., Clark, R. W., Rosenzweig, S. E., and Blake, W. B., "Summary of Flight Testing and Results for the Formation Flight for Aerodynamic Benefit Program," AIAA 2014-1457, Proceedings of 52nd Aerospace Sciences Meeting, National Harbor, MD, January 13-17, 2014. DOI: 10.2514/6.2014-1457.

[5]Voskuijl, M., "Cruise Range in Formation Flight," *Journal of Aircraft*, Vol. 54, (6), 2017, pp. 1–8. DOI: 10.2514/1.C034246.

[6]Hummel, D., "The Use of Aircraft Wakes to Achieve Power Reductions in Formation Flight," Proceedings of the AGARD FDP Symposium, Trondheim, Norway, May 20–23, 1996, pp. 36-1 to 36-13.

[7]Vachon, M. J., Ray, R. J., Walsh, K. R., and Ennix, K., "F/A-18 Aircraft Performance Benefits Measured during the Autonomous Formation Flight Project," AIAA 2002-4491, Proceedings of the AIAA Atmospheric Flight Mechanics Conference and Exhibit, Monterey, CA, August 5–8, 2002, pp. 1–26, DOI: 10.2514/6.2002-4491.

[8]Wieselberger, C., "Beitrag zur Erlkärung des Winkelfluges einer Zugvogel," *ZFM*, Vol. 5, 1914, pp. 225–229.

[9]Hummel, D., "Recent Aerodynamic Contributions to Problems of Bird Flight," Proceedings of 11th Congress of the International Council of Aeronautical Sciences, Lisbon, Portugal, September 10–16, 1978.

[10]Ning, S. A., Kroo, I., Aftosmis, M. J., Nemec, M., and Kless, J. E., "Extended Formation Flight at Transonic Speeds," *Journal of Aircraft*, Vol. 51, (5), September 2014, pp. 1501–1510. DOI: 10.2514/1.C032385.

[11]Padfield, G. D., and Tuner, G. P., "Helicopter Encounters with Aircraft Vortex Wakes," *The Aeronautical Journal*, 2001, Vol. 105, (1043), pp. 1–8, DOI: 10.1017/S0001924000095920.

[12]Lawrence, B., Padfield, G. D., and Taghizad, A., "Rotorcraft Wake Vortex Encounters: A Flight Mechanics Perspective," Proceedings of the 32nd European Rotorcraft Forum, Maastricht, The Netherlands, September 12–16, 2006, pp. 1–32.

[13]Lawrence, B., and Padfield, G. D., "Wake Vortex Encounter Severity for Rotorcraft in Approach and Landing," Proceedings of the 31st European Rotorcraft Forum, Florence, Italy, September 13–15, 2005, pp. 1–16.

[14]Padfield, G. D., Manimala, B., and Turner, G. P., "A Severity Analysis for Rotorcraft Encounters with Vortex Wakes," *Journal of the American Helicopter Society*, Vol. 49, (4), 2004, pp. 445–456.

[15]Matayoshi, N., and Okuno, Y., "Evaluation of Helicopter Encounters with Wake Vortices," Proceedings of the 35th European Rotorcraft Forum, Hamburg, Germany, September 22–25, 2009, pp. 1–12.

[16]Johnson, W., Yamauchi, G. K., Derby, M. R., and Wadcock, A. J., "Wind Tunnel Measurements and Calculations of Aerodynamic Interactions between Tiltrotor Aircraft," AIAA 2003-47, Proceedings of the 41st AIAA Aerospace Sciences Meeting and Exhibit, Reno, NV, January 6–9, 2003, pp. 1–10. DOI: 10.2514/6.2003-47.

[17]Romander, E., Betzina, M., Silva, M., Wadcock, A., and Yamauchi, G., "Investigating Tiltrotor Formation Flight via 1/48-Scale Wind Tunnel Experiment," Proceedings of the 62nd Annual Forum of the American Helicopter Society, Phoenix, AZ, May 9–11, 2006, pp. 1–19.

[18]Yamauchi, G. K., Wadcock, A. J., and Derby, M. R., "Measured Aerodynamic Interaction of Two Tiltrotors," Proceedings of the 59th Annual Forum of the American Helicopter Society, Phoenix, AZ, May 6–8, 2003, pp. 1720–1731.

[19]Silva, M. J., Wachspress, D. A., Gaublomme, D. P., Hayden, E. W., Davis, T. S., and Fean, T. G., "The Role of Modeling & Simulation in the Mitigation of V-22 Tiltrotor Formation Flight Wake-Induced Roll-off," Proceedings of the 72nd Annual Forum of the American Helicopter Society, West Palm Beach, FL, May 16–19, 2016, pp. 2424–2440.

[20]Yemenici, O., Sezer-Uzol, N., and Uzol, O., "Investigation of Rotor-Rotor Interactions for Two Helicopters in Forward Flight Using Free-Vortex Wake Methodology," AIAA 2010-4558, Proceedings of the 28th AIAA Applied Aerodynamics Conference, Chicago, IL, June 28–July 1, 2010. DOI: 10.2514/6.2010-4558.

[21]Heyson, H. H., "Preliminary Results from Flow-Field Measurements around Single and Tandem Rotors in the Langley Full-Scale Tunnel," NACA TN-3242, 1954.

[22]Heyson, H. H., and Katzoff, S., "Induced Velocities near a Lifting Rotor with Non-Uniform Disk Loading," NACA Report 1319, 1957.

[23]Egolf, T. A., "An Analytical and Experimental Study of Farfield Rotor Wake Geometry and Velocity," M.Sc. Thesis, Pennsylvania State University, 1973.

[24]Rajagopalan, R. G., and Mathur, S. R., "Three Dimensional Analysis of a Rotor in Forward Flight," *Journal of the American Helicopter Society*, Vol. 38, (3), July 1993, pp. 14–25. DOI: 10.4050/JAHS.38.14.

[25]Caprace, D.-G., Buffin, S., Duponcheel, M., Chatelain, P., and Winckelmans, G., "Large Eddy Simulation of Advancing Rotor for Near to Far Wake Assessment," Proceedings of the 43rd European Rotorcraft Forum, Milan, Italy, September 12–15, 2017.

[26]FOX 52, "UH-60A Blackhawk Illustration," available at `https://commons.wikimedia.org/w/index.php?curid=44705055`, accessed May 2019; CC BY-SA 4.0.

[27]Howlett, J., "UH-60A Black Hawk Engineering Simulation Program: Volume I – Mathematical Model," NASA CR-66309, 1981.

[28]Howlett, J., "UH-60A Black Hawk Engineering Simulation Program: Volume II – Background Report," NASA CR-166310, 1988.

[29]Ballin, M. G., "Validation of a Real-Time Engineering Simulation of the UH-60A Helicopter," NASA TM-88360, 1987.

[30]Buckanin, R. M., Reynolds, T. L., Kelly, W. A., Lockwood, R. A., Webre, J. L., and Cason, R. W., "Level Flight Performance Evaluation of the UH-60A Helicopter with the Production External Stores Support System and Ferry Tanks Installed," Final Report, AEFA Project No. 86-01, 1986.

[31]Voskuijl, M., Van Bruchem, B.-J., and Van Liempt, M., "Helicopter Drive Train Load Alleviation in Hover by Nonlinear Control," Proceedings of the 74th Annual Forum & Technology Display of the American Helicopter Society, Phoenix, AZ, May 14–17, 2018.

[32]Pastorelli, S., Battezzato, A., and Mattiazzo, G., "Flyby-Wire Control of a Helicopter: Multibody Main Rotor Model," Proceedings of the 26th Congress of International Council of the Aeronautical Sciences, Anchorage, AK, September 14–19, 2008.

[33]Peters, D. A., and He, C. J., "Finite State Induced Flow, Part II: Three-Dimensional Rotor Disk," *Journal of Aircraft*, Vol. 32, (2), 1995, pp. 323–333(11). DOI: 10.2514/3.46719.

[34]Peters, D. A., and He, C. J., "Correlation of Measured Induced Velocities with a Finite-State Wake Model," *Journal of the American Helicopter Society*, Vol. 36, (3), 1991, pp. 59–70.

[35]Hilbert, K. B., "A Mathematical Model of the UH60 Helicopter," NASA TM-85890, 1984.

[36]Totah, J., "A Critical Assessment of UH-60 Main Rotor Blade Airfoil Data," NASA TM-103985, 1993.

[37]Du Val, R. W., "A Real-Time Multi-Body Dynamics Architecture for Rotorcraft Simulation," Proceedings of the Challenge of Realistic Rotorcraft Simulation, RAeS, London, UK, November 7–8, 2001.

[38]He, C. J., and Du Val, R. W., "An Unsteady Airload Model with Dynamic Stall for Rotorcraft Simulation," Proceedings of the 50th Annual Forum of the American Helicopter Society, Washington, DC, May 11–13, 1994, pp. 931–949.

[39]Baskin, V. E., Vil'dgrube, L. S., Vozhdayev, Y. S., and Maykapar, G. I., "Theory of the Lifting Airscrew," NASA TT-F-823, 1976.

[40]Wilson, J. C., "User's Guide For A Flat Wake Rotor Inflow/Wake Velocity Prediction Code, DOWN," NASA TM-104139, 1991.

[41]Wilson, J. C., "Experimental Evaluation of a Flat Wake Theory for Predicting Rotor Inflow-Wake Velocities," NASA AVSCOM TM-4334, 1992.

[42]Whitehouse, G. R., and Brown, R. E., "Modeling the Mutual Distortions of Interacting Helicopter and Aircraft Wakes," *Journal of Aircraft*, Vol. 40, (3), 2003, pp. 440–449. DOI: 10.2513/2.3139.

[43]Schaeffler, N. W., Allan, B. G., Lienard, C., and Le Pape, A., "Progress towards Fuselage Drag Reduction via Active Flow Control: A Combined CFD and Experimental Effort," Proceedings of the 36th European Rotorcraft Forum, Paris, France, September 7–9, 2010, pp. 064.1–064.17.

[44]Takahashi, M. D., "A Flight-Dynamic Helicopter Mathematical Model with a Single Flap-Lag-Torsion Main Rotor," NASA TM-102267, 1990.

[45]Veldhuis, L., Voskuijl, M., and Fransen, B., "Formation Flight – Fine-Tuning of Theoretical Performance Prediction," AIAA 2013-0961, Proceedings of the 51st AIAA Aerospace Sciences Meeting Including the New Horizons Forum and Aerospace Exposition, Grapevine, TX, January 7–10, 2013. DOI: 10.2514/6.2013-961.

[46]Prouty, R. W., *Helicopter Performance, Stability, and Control*, Fourth edition, Krieger Publishing Company, Malabar, FL, 2002, Chapter 3.